Precision test of the SM with Kl2, Kl3 decays at the KLOE experiment

T. Spadaro[a*]

[a]Laboratori Nazionali di Frascati INFN, Via E. Fermi, 40, 00044, Frascati, Italy.

A brief description of the physics implications of the KLOE measurements of $K \to l\nu_l(\gamma)$ (K_{l2}) and $K \to \pi l\nu_l(\gamma)$ (K_{l3}) decays is given. Particular emphasis is put on the measurement of the ratio of K_{e2} and $K_{\mu 2}$ BR's: the status of the analysis and present and future sensitivity to physics beyond the SM are discussed.

1. The KLOE legacy

New precise measurements of $K \to l\nu_l(\gamma)$ (K_{l2}) and $K \to \pi l\nu_l(\gamma)$ (K_{l3}) decays can possibly shed light on new physics (NP). The first indication of the need of improving the present knowledge in this field was given by the 2004 version of the PDG: a deviation from unitarity of the CKM matrix was observed in the first row, amounting to more than two standard deviations [1],

$$\Delta = 1 - V_{ud}^2 - V_{us}^2 - V_{ub}^2 = 0.0043(16)_{Vud}(11)_{Vus}. \quad (1)$$

This called for new precise determinations of the V_{us} parameter of the CKM matrix, traditionally extracted from K_{l3} decays using the following expression:

$$\Gamma^i(K_{e3(\gamma),\,\mu 3(\gamma)}) = |V_{us}|^2 \frac{C_i^2 G^2 M^5}{128\pi^3} S_{\rm EW} |f_+^{K^0}(0)|^2 I^i_{e3,\,\mu 3}\,(1+\delta^i_{e3,\,\mu 3}),$$

where i indexes $K^0 \to \pi^-$ and $K^+ \to \pi^0$ transitions for which $C_i^2 = 1$ and $1/2$, respectively, G is the Fermi constant, M is the appropriate kaon mass, and $S_{\rm EW}$ is a universal short-distance electroweak correction [2]. The δ^i term accounts for long-distance radiative corrections depending on the meson charges and lepton masses and, for $K^\pm$, for isospin-breaking effects. These corrections are presently known at the few-per-mil level [3]. The $f_+^{K^0}(0)$ form factor parametrizes the vector-current transition $K^0 \to \pi^-$ at zero momentum transfer t, while the dependence of vector and scalar form factors on t enter into the determination of the integrals $I_{e3,\,\mu 3}$ of the Dalitz-plot density over the physical region.

After four years of analysis of KLOE data, we present the most comprehensive set of results from a single experiment, including BR's for K_{e3} and $K_{\mu 3}$ decays for K_L [4] and $K^\pm$ [5], and the BR for $K_S \to \pi e\nu$ [6, 7] (unique to KLOE); form factor slopes from analysis of K_{Le3} [8] and $K_{L\mu 3}$ [9]; lifetime measurements for K_L [10] and $K^\pm$ [11]; the K^0 mass [12]. Using the K_S lifetime from PDG [13] as the only input other than KLOE measurements, we obtain five results for the product $f_+(0)|V_{us}|$ [14]:

Mode	$f_+ \times \lvert V_{us}\rvert$	Error,%
K_{Le3}	0.2155(7)	0.3
$K_{L\mu 3}$	0.2167(9)	0.4
K_{Se3}	0.2153(14)	0.7
$K^\pm_{e3}$	0.2152(13)	0.6
$K^\pm_{\mu 3}$	0.2132(15)	0.7

(2)

The average of these results has been obtained taking all correlations into account and it is $f_+(0) \times |V_{us}| = 0.2157(6)$. From this, using $f_+(0) = 0.9644(49)$ from the UKQCD/RBC collaboration [15], we obtain

$$|V_{us}| = 0.2237(13). \quad (3)$$

Using the V_{ud} world average from $0^+ \to 0^+$ nuclear β decays [16],

$$V_{ud} = 0.97418(26), \quad (4)$$

CKM unitarity can be seen to be satisfied: $\Delta = 9(8) \times 10^{-4}$.

*For the KLOE collaboration, author list can be seen at `www.lnf.infn.it/kloe/kloe_authors.ps`

KLOE has provided the most precise determination of the $K_{\mu 2}$ BR [17], which can be linked to the ratio V_{us}/V_{ud} via the following relation [18]:

$$\frac{\Gamma(K \to \mu\nu)}{\Gamma(\pi \to \mu\nu)} = \frac{m_K \left(1 - m_\mu^2/m_K^2\right)^2}{m_\pi \left(1 - m_\mu^2/m_\pi^2\right)^2} \left|\frac{V_{us}}{V_{ud}}\right|^2 \frac{f_K^2}{f_\pi^2} C.$$

The theoretical inputs are the form-factor ratio f_K/f_π and the radiative corrections described by the factor C. We use $f_K/f_\pi = 1.189(7)$ from lattice calculations by the HP/UKQCD collaboration [19], and $C = 0.9930(35)$ from [18], thus obtaining

$$|V_{us}/V_{ud}| = 0.2326(15). \quad (5)$$

From the KLOE results of Eqs 3 and 5, and from V_{ud} of Eq. 4, a combined fit to V_{us} and V_{ud} has been done. The result is shown in Fig. 1: the fit χ^2 is 2.34 for one degree of freedom (13% probability) and the results are:

$$|V_{us}| = 0.2249(10) \text{ and } |V_{ud}| = 0.97417(26), \quad (6)$$

with a correlation of 3%. From these, not only can we now state that the CKM unitary holds to within 10^{-3},

$$\Delta = 0.0004 \pm 0.0005_{Vud} \pm 0.0004_{Vus}, \quad (7)$$

but we can also translate this experimental result into a severe constraint for many NP models: SM extensions predicting gauge universality breaking of weak decays (the weak coupling constant G_F from μ lifetime would then be different from the one, G_{CKM}, extracted from quark decays) are constrained to have high mass mediators [20]. Generally speaking, a measurement of $G_{CKM} \sim G_F(|V_{ud}^2| + |V_{us}^2|)$ with a 0.5% error is sensitive to NP mediators with a mass of less than $\sim$13 TeV (~ 1) TeV, provided they are exchanged at tree (loop) level diagrams. With the present accuracy, the information from G_{CKM} is more constraining than that coming from τ decays and electro-weak precision tests [21].

Measurements of K_{l2} widths can be linked to new physics effects, too. The ratio of $K_{\mu 2}$ to $\pi_{\mu 2}$ decay widths might accept NP contributions from charged Higgs exchange [22, 23] in supersymmetric extensions of the SM with two Higgs doublets. The effect would be a difference of the V_{us}/V_{ud} ratio extracted from $K_{\mu 2}$, $\pi_{\mu 2}$ and that extracted from K_{l3} and superallowed Fermi transitions ("0^+"):

$$\left|\frac{V_{us}(K_{l2})V_{ud}(0^+)}{V_{us}(K_{l3})V_{ud}(\pi_{l2})}\right| = \left|1 - \frac{m_K^2(m_s - m_d)\tan^2\beta}{M_H^2 m_s(1 + \epsilon_0 \tan\beta)}\right|,$$

where $\tan\beta$ is the ratio of up- and down-Higgs vacuum expectation values, M_H is the charged Higgs mass, and $\epsilon_0 \sim 0.01$ [24]. The KLOE result of this ratio can be translated into an 95%-CL exclusion plot in the plane $\tan\beta$ vs M_H (see Fig. 2), showing that this analysis is complementary to and competitive with that [23] using the average $\mathrm{BR}(B \to \tau\nu) = 1.42(44) \times 10^{-4}$ of Babar and Belle measurements [25].

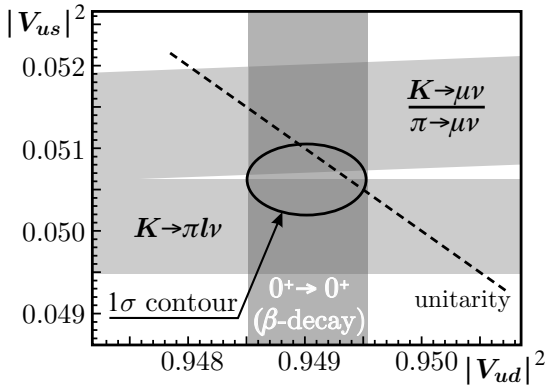

Figure 1. The 1-σ fit result to V_{ud} and V_{us} is shown by the solid line ellipse, in agreement with the unitarity bound shown by the dashed line.

A strong interest for a new measurement of the ratio $R_K = \Gamma(K^\pm \to e^\pm\bar{\nu_e})/\Gamma(K^\pm \to \mu^\pm\bar{\nu_\mu})$ has recently arisen, triggered by the work of Ref. 26.

The SM prediction of R_K benefits from cancellation of hadronic uncertainties to a large extent and therefore can be calculated with high precision. Including radiative corrections, the total uncertainty is less than 0.5 per mil [27]. Since the electronic channel is helicity-suppressed by the $V - A$ structure of the charged weak current, R_K can receive contributions from physics beyond the SM, for example from multi-Higgs effects inducing an effective pseudoscalar interaction. It has

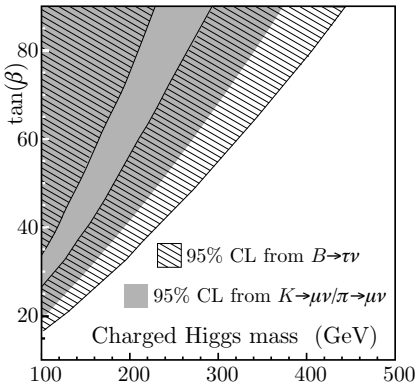

Figure 2. Excluded regions at 95% CL from analysis of decays $K \to \mu\nu$ (filled area) and $B \to \tau\nu$ (hatched area).

been shown in Ref. 26 that deviations from the SM of up to few percent on R_K are quite possible in minimal supersymmetric extensions of the SM and in particular should be dominated by lepton-flavor violating contributions with tauonic neutrinos emitted. Using the present KLOE dataset of ∼2.5 fb^{-1} of luminosity integrated at the ϕ-meson peak, we show that an accuracy of about 1 % in the measurement of R_K might be reached.

In order to compare with the SM prediction at this level of accuracy, one has to treat carefully the effect of radiative corrections, which contribute several percent to the K_{e2} width. In particular, the SM prediction of Ref. [27] is made considering all photons emitted by the process of internal bremsstrahlung (IB) while ignoring any contribution from structure-dependent direct emission (DE). Of course both processes contribute, so in the analysis we will consider DE as a background which can be distinguished from the IB width by means of a different photon energy spectrum. The analysis of $K_{e2}/K_{\mu 2}$ will be the main topic discussed here.

2. The KLOE setup

DAΦNE, the Frascati ϕ factory, is an e^+e^- collider working at $\sqrt{s} \sim m_\phi \sim 1.02$ GeV. ϕ mesons are produced, essentially at rest, with a visible cross section of ~ 3.1 μb and decay into K^+K^- pairs with a BR of $\sim 49\%$.

Kaons get a momentum of ~ 100 MeV/c which translates into a low speed, $\beta_K \sim 0.2$. K^+ and K^- decay with a mean length of $\lambda_\pm \sim 90$ cm and can be distinguished from their decays in flight to one of the two-body final states $\mu\nu$ or $\pi\pi^0$.

The kaon pairs from ϕ decay are produced in a pure $J^{PC} = 1^{--}$ quantum state, so that observation of a K^+ in an event signals, or tags, the presence of a K^- and vice versa; highly pure and nearly monochromatic $K^\pm$ beams can thus be obtained and exploited to achieve high precision in the measurement of absolute BR's [5, 17]

The analysis of kaon decays is performed with the KLOE detector, consisting essentially of a drift chamber, DCH, surrounded by an electromagnetic calorimeter, EMC. A superconducting coil provides a 0.52 T magnetic field. The DCH [28] is a cylinder of 4 m in diameter and 3.3 m in length, which constitutes a fiducial volume for $K^\pm$ decays extending for $\sim 1\lambda_\pm$, respectively. The momentum resolution for tracks at large polar angle is $\sigma_p/p \leq 0.4\%$. The c.m. momenta reconstructed from identification of 1-prong $K^\pm \to \mu\nu, \pi\pi^0$ decay vertices in the DC peak around the expected values with a resolution of 1–1.5 MeV, thus allowing clean and efficient $K^\mp$ tagging.

The EMC is a lead/scintillating-fiber sampling calorimeter [29] consisting of a barrel and two endcaps, with good energy resolution, $\sigma_E/E \sim 5.7\%/\sqrt{\mathrm{E(GeV)}}$, and excellent time resolution, $\sigma_T = 54$ ps$/\sqrt{\mathrm{E(GeV)}} \oplus 50$ ps. The timing capabilities of the EMC are exploited to precisely reconstruct the position of decay vertices of $K^\pm$ to π^0's from the cluster times of the emitted photons, thus allowing a precise measurement of the $K^\pm$ lifetime [11].

In early 2006, the KLOE experiment completed data taking, having collected ~ 2.5 fb^{-1} of integrated luminosity at the ϕ peak, corresponding to ∼3.6 billion K^+K^- pairs.

3. Event selection

Given the $K^\pm$ decay length of ∼90 cm, the selection of one-prong $K^\pm$ decays in the DC required to tag $K^\mp$ has an efficiency smaller than 50%. In order to keep the statistical uncertainty on the number of $K^\pm \to e^\pm\bar{\nu}_e$ counts below

1%, we decided to perform a "direct search" for $K^\pm \to e^\pm\bar{\nu_e}$ and $K^\pm \to \mu^\pm\bar{\nu_\mu}$ decays, without tagging. Since we measure a ratio of BR's for two channels with similar topology and kinematics, we expect to benefit from some cancellation of the uncertainties on tracking, vertexing, and kinematic identification efficiencies. Small deviations in the efficiency due to the different masses of e's and μ's can be evaluated using MC.

Selection starts requiring a kaon track decaying in a DC fiducial volume (FV) with laboratory momentum between 70 and 130 MeV, and a secondary track of relatively high momentum (above 180 MeV). The FV is defined as a cylinder parallel to the beam axis with length of 80 cm, and inner and outer radii of 40 and 150 cm, respectively. Quality cuts are applied using χ^2-like variables for the tracking of kaon and secondary particle and for the vertex fit. These requirements are referred to as the "one-prong selection" in the following.

A powerful kinematic variable used to distinguish $K^\pm \to e^\pm\bar{\nu_e}$ and $K^\pm \to \mu^\pm\bar{\nu_\mu}$ decays from the background is calculated from the momenta of the kaon and the secondary particle measured in DC: assuming zero neutrino mass one can obtain the squared mass of the secondary particle, or lepton mass ($M^2_{\rm lep}$). The distribution of $M^2_{\rm lep}$ is shown in Fig. 3 for MC events before and after quality cuts are applied. While the one-prong selection is enough for clean identification of a $K^\pm \to \mu^\pm\bar{\nu_\mu}$ sample, further rejection is needed in order to identify $K^\pm \to e^\pm\bar{\nu_e}$ events: the background, which is dominated by badly reconstructed $K^\pm \to \mu^\pm\bar{\nu_\mu}$ events, is reduced by a factor of $\sim$10 by the quality cuts, but still remains $\sim$10 times more frequent than the signal in the region around the electron mass peak. The one-prong selection efficiency is $\sim 28\%$ for both channels, and the ratio of efficiencies for $K^\pm \to \mu^\pm\bar{\nu_\mu}$ and $K^\pm \to e^\pm\bar{\nu_e}$ is evaluated from MC to be: $\epsilon^{\rm TRK}_{K\mu 2}/\epsilon^{\rm TRK}_{Ke2} = 0.974(1)$. A correction to this estimate accounting for possible differences in the tracking performance between data and MC is discussed in Sec. 5.

Information from the EMC is used to improve background rejection. The secondary track is extrapolated to a position $\vec{r}_{\rm ext}$ on the EMC surface with momentum $\vec{p}_{\rm ext}$ and associated to

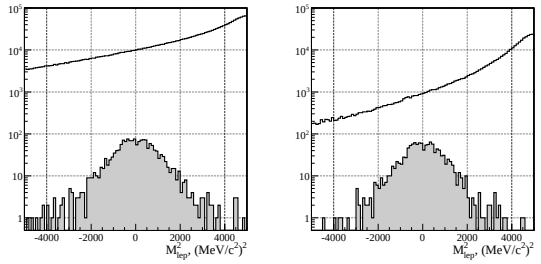

Figure 3. MC distribution of $M^2_{\rm lep}$ before (left) and after (right) quality cuts are applied. Shaded histogram: $K^\pm \to e^\pm\bar{\nu_e}$ events. Open histograms: background, dominated by $K^\pm \to \mu^\pm\bar{\nu_\mu}$ events. In MC, R_K is set to the SM value.

nearest calorimeter cluster satisfying the impact-parameter cut $d_\perp < 30$ cm, where $d_\perp = |\vec{p}_{\rm ext}/|p_{\rm ext}| \times (\vec{r}_{\rm ext} - \vec{r}_{\rm cl})|$. For electrons, the associated cluster is close to the EMC surface so that its position projected along the track $d_\parallel = |\vec{p}_{\rm ext} \cdot (\vec{r}_{\rm ext} - \vec{r}_{\rm cl})|$ is only a few cm. Moreover, for electrons the cluster energy $E_{\rm cl}$ is a measurement of the particle momentum $p_{\rm ext}$. Therefore the following condition is required in the plane $E_{\rm cl}/p_{\rm ext}$ vs $d_\parallel$ (see Fig. 4):

$$\left(\frac{d_\parallel[\rm cm] - 2.6}{2.6}\right)^2 + \left(\frac{E_{\rm cl}/p_{\rm ext} - 0.94}{0.2}\right)^2 < 2.5. \quad (8)$$

Electron clusters can be further distinguished from μ (or π) clusters by exploiting the granularity of the EMC: electrons shower deposits their energy mainly in the first plane of EMC, while muons behave like minimum ionizing particles in the first plane and they deposit a sizable fraction of their kinetic energy from the third plane onward when they are slowed down to rest (Bragg peak). The particle identification (PID) was therefore based on the asymmetry A_f of energy deposits between the second and the first planes hit, on the spread $E_{\rm RMS}$ of energy deposits on each plane, on the position $r_{\rm max}$ of the plane with the maximum energy, and on the asymmetry A_l of energy deposits between the last and the next-to-last planes. Muon clusters with the signature $A_f > 0$, or $x_{\rm max} > 12$ cm, or $A_l < -0.85$ are rejected. This criteria were optimized during MC and control sample studies.

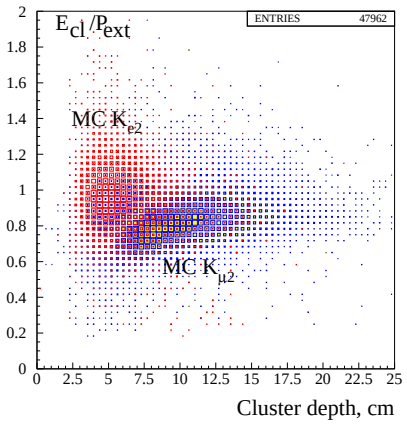

Figure 4. MC distribution of the ratio $E_{\rm cl}/P_{\rm ext}$ of cluster energy and track momentum as a function of the depth of the cluster along the direction of impact of the secondary particle on the EMC.

The PID technique described above selects $K^{\pm} \to e^{\pm}\bar{\nu_e}$ events with an efficiency $\epsilon^{\rm PID}_{Ke2} \sim 64.7(6)\%$ and a rejection power for background of ~ 300. These numbers have been evaluated from MC. The effect of the improvement in background rejection obtained with PID is visible by comparing $M^2_{\rm lep}$ distributions before and after the PID is applied; see Fig. 5.

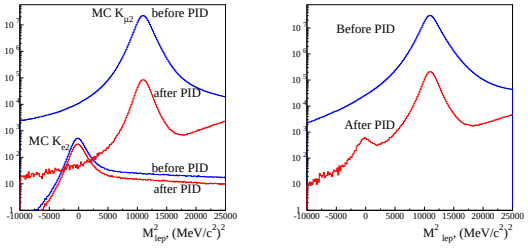

Figure 5. Left: MC distribution of $M^2_{\rm lep}$ for background (plots with larger population) and for signal (lower populations) before and after the PID is required. Right: data distribution of $M^2_{\rm lep}$ before and after the PID is required. The $K^{\pm} \to e^{\pm}\bar{\nu_e}$ signal is visible only after PID.

4. Event counting

A likelihood fit to the two-dimensional $E_{\rm RMS}$ vs $M^2_{\rm lep}$ distribution was performed to get the number of signal events. Distribution shapes for signal and background were taken from MC; the normalizations for the two components are the only fit parameters. The number of signal events obtained from the fit is $N_{Ke2} = 8090 \pm 156$. Projections of the fit results onto the two axes are compared to real data in Fig. 6.

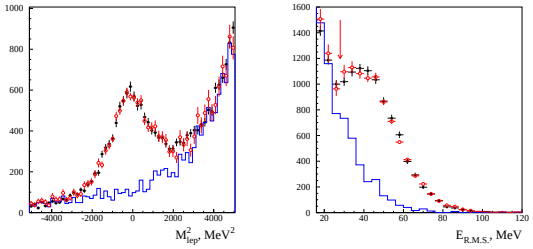

Figure 6. Distributions of the lepton mass squared $E^2_{\rm lep}$ of the secondary track (left panel) and of the spread $E_{\rm RMS}$ of the energy deposits among the planes of the connected cluster in the EMC (right panel). Filled dots represent the data, open dots are the result of a maximum-likelihood fit using signal and background (solid line) distributions as input.

The primary generators for $K^{\pm} \to e^{\pm}\bar{\nu_e}$ and $K^{\pm} \to \mu^{\pm}\bar{\nu_\mu}$ decays include radiative corrections and allow for the emission of a single photon in the final state [30]. $K^{\pm} \to e^{\pm}\bar{\nu_e} + \gamma$ events with photon energy in the kaon rest frame $E_\gamma < 20$ MeV were considered as signal: as shown in Fig. 7, the DE contribution is indeed negligible in this range. The fraction of the IB component lying in the chosen energy range is determined from MC to be $\epsilon^{\rm IB} = 0.9528(5)$.

While evaluating the shape for $K \to e\nu(\gamma)$, the present PDG value has been used for the ratio of IB and DE contributions: IB/(IB + DE) = 0.50(4) [13]. The fit has been repeated with different values of this ratio, varied within its range of uncertainty. This procedure gave a $\sim$0.45%

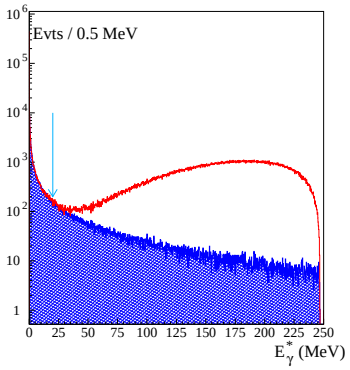

Figure 7. Distribution of the energy of the emitted photon in a $K \to e\nu\gamma$ decay, from the inner bremsstrahlung width (hatched histogram) or through the total inner bremsstrahlung + direct emission processes.

error on the number of signal counts.

The number of $K^\pm \to \mu^\pm\bar{\nu_\mu}$ events in the same data set is extracted from a similar fit to the $M^2_{\rm lep}$ distribution, where no PID cuts are applied in this case. The fraction of background events under the muon peak is estimated from MC to be less than one per mil. The number of $K^\pm \to \mu^\pm\bar{\nu_\mu}$ events is 499 251 584±35403.

5. Evaluation of R_K

The following formula has been used to evaluate the ratio R_K:

$$R_K = \frac{N_{Ke2}}{N_{K\mu 2}} \left(\frac{\epsilon^{\rm TRG}_{K\mu 2}}{\epsilon^{\rm TRG}_{Ke2}}\right) \left(\frac{\epsilon^{\rm TRK}_{K\mu 2}}{\epsilon^{\rm TRK}_{Ke2}}\right) \left(\frac{C^{\rm TRK}}{C^{\rm PID}\epsilon^{\rm PID}_{Ke2}}\right) \frac{1}{\epsilon^{\rm IB}},$$

where N_{Ke2} and $N_{K\mu 2}$ are the number of $K^\pm \to e^\pm\bar{\nu_e}$ and $K^\pm \to \mu^\pm\bar{\nu_\mu}$ observed events; $\epsilon^{\rm TRK}_{Ke2}$ and $\epsilon^{\rm TRK}_{K\mu 2}$ are the efficiencies for the one-prong selection for $K^\pm \to e^\pm\bar{\nu_e}$ and $K^\pm \to \mu^\pm\bar{\nu_\mu}$ decays, evaluated from MC; the correction $C^{\rm TRK}$ to their ratio accounts for possible differences between the data and the MC prediction. The PID efficiency for $K^\pm \to e^\pm\bar{\nu_e}$ events $\epsilon^{\rm PID}_{Ke2}$ has been evaluated from MC, while a correction $C^{\rm PID}$ has been evaluated to account for possible discrepancies between data and MC in the description of PID variables. Trigger efficiencies $\epsilon^{\rm TRG}$ were instead evaluated directly from data. Finally, $\epsilon^{\rm IB}$ is the fraction of the IB component accepted in the selection of $K^\pm \to e^\pm\bar{\nu_e}$ events and has been evaluated from MC.

The MC estimates for $\epsilon^{\rm TRK}$ have been checked using a control sample of $K^\pm \to \mu^\pm\bar{\nu_\mu}$ events. The correction is $C_{\rm TRK} = 0.994(9)$, where the error is purely statistical. In order to check the reliability of the MC for the PID efficiency estimate, a control sample (CS) of K_{Le3} decays has been selected and used to compare data with MC. The correction is $C^{\rm PID} = 1.009 \pm 0.009 \pm 0.015$, where the first error is due to the statistics and the second is due to the incomplete kinematic coverage of the CS. The trigger efficiencies for $K^\pm \to e^\pm\bar{\nu_e}$ and $K^\pm \to \mu^\pm\bar{\nu_\mu}$ are evaluated from data, by comparing two almost independent trigger algorithms based on DC and EMC information. The result is $\epsilon^{\rm TRG}_{K\mu 2}/\epsilon^{\rm TRG}_{Ke2} = 0.998 \pm 0.009 \pm 0.006$, where again the first and second errors are statistical and systematic, respectively. The estimates of the above efficiencies and corrections are discussed in detail elsewhere [31].

Using the number of observed $K^\pm \to e^\pm\bar{\nu_e}$ and $K^\pm \to \mu^\pm\bar{\nu_\mu}$ events and all corrections, we get the preliminary result

$$R_K = (2.55 \pm 0.05 \pm 0.05) \times 10^{-5}. \qquad (9)$$

This value is compatible within the error with the SM prediction, $R_K = (2.477 \pm 0.001) \times 10^{-5}$, and with other recent measurements by NA48 [32].

6. Prospects: analysis improvements

Three sources contribute to the present statistical uncertainty of 1.9%: fluctuation in the signal counts (1.1%), fluctuation in the background to be subtracted (0.7%), and statistical error on the MC estimate of the background (1.4%). The dominant source is the latter, because the selection efficiency for badly reconstructed $K^\pm \to \mu^\pm\bar{\nu_\mu}$ events is lower in MC than in data, so that the MC background under the $K^\pm \to e^\pm\bar{\nu_e}$ peak (the solid histogram of Fig. 6) had to be scaled by a factor of 4 to match the level of background in data.

Two improvements have been implemented to lower the statistical uncertainty on R_K: first, a

new MC production allowed the statistics to be increased by a factor of two; second, various improvements have been performed to the selection algorithm in order to increase the background rejection power.

A better parametrization of kinematic criteria has been applied. The expected error on the $M^2_{\rm lep}$ variable was used in the analysis presented as indicator of the quality of the tracking. This variable depends on the K-lepton opening angle $\cos\theta$. Since K_{e2} and $K_{\mu 2}$ decays have different $\cos\theta$ distributions, a trailing 2-σ cut on the distribution of the error has been applied: this allows higher rejection to be achieved, maintaining an accurate cancellation of the associated efficiency among the two channels.

Moreover, a redundant determination of the K momentum has been exploited to further reduce the $K_{\mu 2}$ background: the kaon track has been extrapolated back to the interaction point, taking the energy lost in the traversed materials into account; the angle between the measured kaon momentum P_{meas} and the ϕ momentum has been used to calculate the expected kaon momentum P_{pred} from the knowledge the $\sqrt{s}$. A cut on the difference of the two determinations improves further the background rejection.

The uncertainty on the PID efficiency is 1.75% and is the dominant contribution to the present systematic error. The CS statistics has been improved by a factor of four and additional studies of PID methods have been performed. Instead of cutting as in Eq. 8, 12 discriminating variables based on EMC information have been used to train a neural network (NN) algorithm. The difference δt of time of flight measured from the associated cluster and predicted from kaon and lepton track lengths has been included in the NN. The NN has been trained as a function of the lepton momentum and the impact angle on the EMC. The NN output for data is compared to the MC using the K_{Le3} control sample and a very good agreement is observed. Semileptonic decays of the K^+ have been also used for that purpose; contrary to the case of K_{Le3}, K^+_{e3} decays allow δt to be calculated exactly as is done for the K_{e2} sample.

No cut has been applied on the NN output: the only PID cut applied in the updated analysis requires a cluster connected to the lepton track with energy above 50 MeV. The systematic error related to this PID selection is therefore reduced, passing from 1.5% to $\sim$ 0.2%. The NN output has been left for fitting the number of K_{e2} events. The data distribution is shown in Fig. 8, while the projections of the fit results are shown in Fig. 9

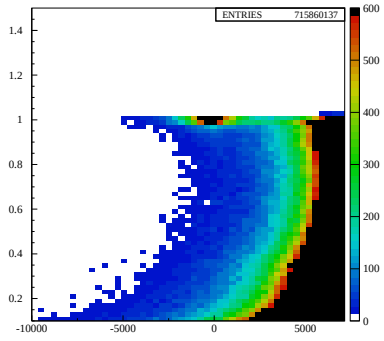

Figure 8. Distribution of the NN output as a function of the lepton mass squared (MeV^2). The plot includes both kaon charges and the entire data set.

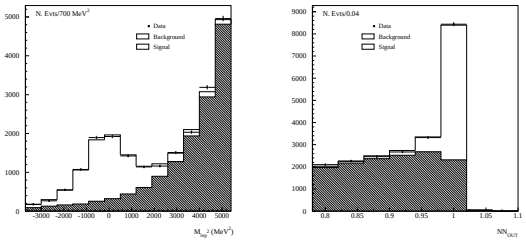

Figure 9. Left (right): M^2_{lep} (NN output) distributions. Data from K^+ decays (dots) and the result of a MC fit (solid histogram) including signal and background (hatched histogram) are shown.

The new PID variable guarantees an improvement by $\sim$ 2 of the effective rejection power with

respect to the presented analysis. To exploit this, the kinematic criteria have been loosened. As a result, the number of K_{e2} events counted in the entire statistics is higher by $\sim 30\%$: $N_{Ke2}(K^+) = 6901 \pm 98$ and $N_{Ke2}(K^-) = 6514 \pm 97$. The total statistical error reaches $\sim 1.1\%$.

The uncertainty on the one-prong selection efficiency is 0.9% in the analysis presented and is dominated by the statistics of the control sample used (only 10 pb^{-1}). Using additional statistics this error has been pushed down to 0.1%. Additional studies of the data/MC agreement on trigger variables for reconstructed events have been done in order to increase the statistics of signal events for trigger efficiency evaluation. The total error from this source has been reduced to 0.4%.

The total error on R_K should be reduced to $\sim 1.3\%$ after analysis completion. As a final perspective, the 95% CL exclusion plots implied by the result of Eq. 9 have been compared with that of a result with the same central value and a total error of 1.3%, see Fig. 10.

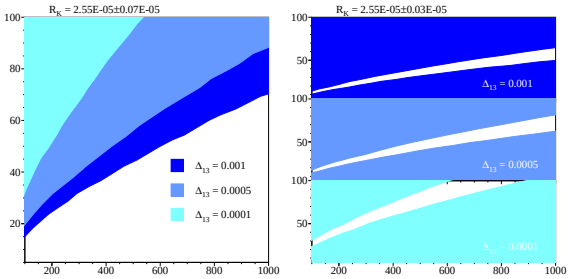

Figure 10. Exclusion plots at 95% CL in the $\tan\beta$-M_H plane from the result of Eq. 9 (left) or from a result with the same central value but a 1.3% error (right). Different values of the Δ_{13} LFV parameter of Ref. 26 are used.

REFERENCES

1. S. Eidelman, *et al.*, *Phys. Lett. B* **592**, 1 (2004).
2. A. Sirlin, *Rev. Mod. Phys.* **50**, 573 (1978); *Nucl. Phys. B* **196**, 83 (1982).
3. V. Cirigliano *et al. Eur. Phys. J. C* **23**, 121 (2002).
4. KLOE Coll., *Phys. Lett. B* **632**, 43 (2006).
5. KLOE Coll., *JHEP* **0802**, 098 (2008).
6. KLOE Coll., *Phys. Lett. B* **636**, 173 (2006).
7. KLOE Coll., *Eur. Phys. J. C* **48**, 767 (2006).
8. KLOE Coll., *Phys. Lett. B* **636**, 166 (2006).
9. KLOE Coll., *JHEP* **0712**, 105 (2008) and arXiv:0707.4631 (2007).
10. KLOE Coll., *Phys. Lett. B* **626**, 15 (2005).
11. KLOE Coll., *JHEP* **0801**, 073 (2008).
12. KLOE Coll., *JHEP* **0712**, 073 (2007).
13. Particle Data Group, W.-M. Yao *et al.*, *J. Phys. G* **33**, 1 (2006).
14. KLOE Coll., *JHEP* **0804**, 059 (2008).
15. RBC/UKQCD Coll., arXiv:0710.5136 (2007).
16. I. S. Towner and J. C. Hardy, arXiv:0710.3181 (2007)
17. KLOE Coll., *Phys. Lett. B* **632**, 76 (2006).
18. W. J. Marciano, *Phys. Rev. Lett.* **93**, 231803 (2004).
19. HPQCD/UKQCD Coll., arXiv:0706.1726 (2007).
20. W. J. Marciano, *Phys. Rev. D* **60**, 093006 (1999).
21. W. J. Marciano, *PoS* **KAON2007**, 003 (2007).
22. W. S. Hou, *Phys. Rev. D* **48**, 2342 (1992).
23. G. Isidori and P. Paradisi, *Phys. Lett. B* **639**, 499 (2006).
24. G. Isidori and A. Retico, *JHEP* **11**, 001 (2001).
25. Belle Coll., *Phys. Rev. Lett.* **97**, 251802 (2006). Babar Coll., arXiv:0705.1820 (2007).
26. A. Masiero, P. Paradisi, and R. Petronzio, *Phys. Rev. D* **74**, 011701 (2006).
27. V. Cirigliano and I. Rosell, arXiv:0707.4464 (2007).
28. KLOE Coll., *Nucl. Instrum. Methods A* **488**, 51 (2002).
29. KLOE Coll., *Nucl. Instrum. Methods A* **482**, 364 (2002).
30. C. Gatti, *Eur. Phys. J. C* **45**, 417 (2005), and references therein.
31. A. Sibidanov, arXiv:0707.4623 (2007).
32. L. Fiorini, *Nucl. Phys. Proc. Suppl.* **169**, 205 (2007);
    V. Kozhuharov, *PoS* **KAON**, 049 (2007).